Aminopolysiloxane as Cu2O Photocathode Overlayer: Photocorrosion Inhibitor and Low Overpotential CO2-to-formate Selectivity Promoter

# Aminopolysiloxane as $Cu_2O$ Photocathode Overlayer: Photocorrosion Inhibitor and Low Overpotential $CO_2$-to-formate Selectivity Promoter

Miguel T. Galante,[a, b] Patrícia V. B. Santiago,[a, b] Victor Y. Yukuhiro,[a, b] Leonardo A. Silva,[a, b] Natália A. Dos Reis,[a, b] Cléo T. G. V. M. T. Pires,[a, b] Nadia G. Macedo,[a, b] Luelc S. Costa,[a, b] Pablo S. Fernandez,*[a, b] and Claudia Longo*[a, b]

$Cu_2O$, a photoactive p-type semiconductor based on earth-abundant elements, shows promising features for photoelectrochemical $CO_2$ reduction reaction (PEC CO2RR). However, despite the broad light absorption and appropriate conduction band edge energy, it promptly undergoes photocorrosion in PEC CO2RR conditions. Herein, we evaluate an amine-functionalized polysiloxane (AF—PSi) as both protective layer and PEC CO2RR promoter via amine-$CO_2$ adduct formation. Electrochemistry experiments and X-ray diffraction showed that photostability is significantly enhanced with AF—PSi overlayer. Electrolyses experiments under visible light irradiation indicated selective production of formate with faradaic efficiency of 61% at low overpotential. Detailed *in situ* FTIR studies revealed that amine groups bind to $CO_2$ to form carbamate species and that this process is favoured by cathodic polarization, confirming the dual role of AF—PSi layer.

Copper (I) oxide is a p-type photoactive semiconductor with a narrow band gap of ~ 2.1 eV. These characteristics, together with the abundance of its constituent elements, makes $Cu_2O$ one of the most thoroughly studied materials for energy-related applications, including solar water splitting[1] and $CO_2$ reduction.[2] Top levels of its valence band (VB) are mainly constituted of Cu-d states, which provides high hole mobility. Its conduction band (CB) edge lies at —1.17 V *vs* RHE at pH = 7,[3] above the thermodynamic potential of many $CO_2$ reduction processes at the same scale/pH. For instance —0.64 V for formate and —0.24 V for methane production,[4] which makes cuprous oxides especially promising for solar fuels production. Despite these interesting features, its wide application in commercial devices and large-scale facilities is still hindered by its prohibitive photoinstability, especially when used as photocathode in aqueous electrolyte-based photoelectrochemical cells, when photocorrosion promptly takes place[5] by either of the following pathways:[6]

$$Cu_2O + H_2O + 2e^- \longrightarrow 2Cu + 2OH^- \quad (1)$$

$$Cu_2O + 2OH^- + 2h^+ \longrightarrow 2CuO + H_2O \quad (2)$$

The origin of both photoactivity/photoinstability of cuprous oxide, as well as, strategies for stabilization can be found in the literature[6] and includes the association with different semiconductors[7,8] or the deposition of protective layers.[9] These strategies provide higher photocurrent and extend the lifetime of $Cu_2O$ electrodes when submitted to cathodic polarization and visible light irradiation. Though valuable information was obtained in recent years, there is still demand for development of novel strategies of $Cu_2O$ PEC enhancement.[10]

In this work, we propose the use of an amine-functionalized polysiloxane (AF—PSi) overlayer for improvement the stability and performance of $Cu_2O$ photocathodes for PEC CO2RR. The enhanced stability was attained due to AF—PSi hydrophobicity, which hindered water-mediated photocorrosion reaction. Also, the AF—PSi performed as a PEC CO2RR promoter, which was achieved by the well-known amine-$CO_2$ adduct formation (Scheme 1), which occurs with species such as heterocyclic amines,[11] superbasic ionic liquids[12-14] and N-containing macromolecules.[15] In this process, as $CO_2$ molecule is converted from its linear form to its bent configuration, the energy barrier for electron transfer to $CO_2$ LUMO is significantly lowered. N-

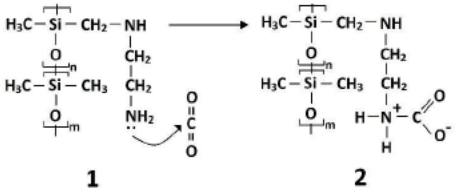


**Scheme 1.** AF—PSi (**1**) reaction with $CO_2$ to form carbamate species (**2**).

[a] *Dr. M. T. Galante, Dr. P. V. B. Santiago, V. Y. Yukuhiro, L. A. Silva, N. A. Dos Reis, Dr. C. T. G. V. M. T. Pires, Dr. N. G. Macedo, Dr. L. S. Costa, Prof. P. S. Fernandez, Prof. C. Longo*
*Institute of Chemistry*
*University of Campinas*
*CEP 13083-970, Campinas (Brazil)*
*E-mail: pablosf@unicamp.br*
*clalongo@unicamp.br*
[b] *Dr. M. T. Galante, Dr. P. V. B. Santiago, V. Y. Yukuhiro, L. A. Silva, N. A. Dos Reis, Dr. C. T. G. V. M. T. Pires, Dr. N. G. Macedo, Dr. L. S. Costa, Prof. P. S. Fernandez, Prof. C. Longo*
*Center for Innovation on New Energies*
*University of Campinas*
*CEP 13083-841, Campinas (Brazil)*

containing polysiloxanes were already shown as efficient $CO_2$ capture agents via N—C bond formation,[16,17] which further supports the strategy presented herein. We selected a commercially available polysiloxane (Dowsil 2-8566, Dow Chemical) which bears —NH—$CH_2$—$CH_2$—$NH_2$ side chains on its polydimethylsiloxane (PDMS) backbone (molecule 1, Scheme 1).

$Cu_2O$ electrodes, obtained by a well-stablished electrodeposition method on glass-FTO,[18] consisted of highly crystalline reddish films with well-defined morphology. These electrodes were covered by a thin layer of AF—PSi (or PDMS) by spin-coating resin solution in THF (Figure S1). Comparison of current-potential profiles obtained by cyclic voltammetry in $CO_2$-saturated aqueous electrolyte (Figure 1a) for the bare and AF—PSi modified $Cu_2O$ electrodes indicated that an additional cathodic process takes place when AF—PSi overlayer is present, which suggests a facilitated charge transfer to $CO_2$ molecules in solution, as already observed with super basic ionic liquids.[12] Remarkable differences were also observed for photovoltage at zero-current potential (ZCP) measurements (Figure 1b). Both electrodes show positive shift in ZCP when illuminated, as expected for p-type semiconductors. However, photovoltage generated at $Cu_2O$—AF—PSi is much higher and stable than that of bare $Cu_2O$. Furthermore, when illumination is interrupted, ZCP of bare $Cu_2O$ electrode shifts to even more positive values before returning to negative potentials, which can indicate major changes in composition of the oxide film due to photocorrosion. Lower photovoltage of photoelectrodes may also indicate occurrence of photocorrosion, in addition to preferential electron-hole recombination rather than faradaic processes.[19] Higher and stable values of photovoltage are of fundamental importance to sustain efficient operation of PEC cells.[20] The incident photon-to-current efficiency (IPCE) curves, measured by polarizing the electrode at —0.30 V (+0,31 V vs RHE) revealed that IPCE values are as much as twice higher when the electrolytic solution is saturated with $CO_2$ (Fig. 1c), indicating that carbon dioxide is involved in faradaic processes at this potential. Furthermore, the observed IPCE values are comparable or even higher than those observed for other copper-based materials in the recent literature.[21-23] Cathodic reactions without $CO_2$ in solution can be associated to $H_2$ evolution, a process well-known to occur at illuminated $Cu_2O$.[24] We stress that no IPCE measurement can be performed at bare $Cu_2O$ electrodes as it readily undergoes photocorrosion, i. e. no stable photocurrent values can be obtained, which in turn would provide a "false positive" IPCE result.

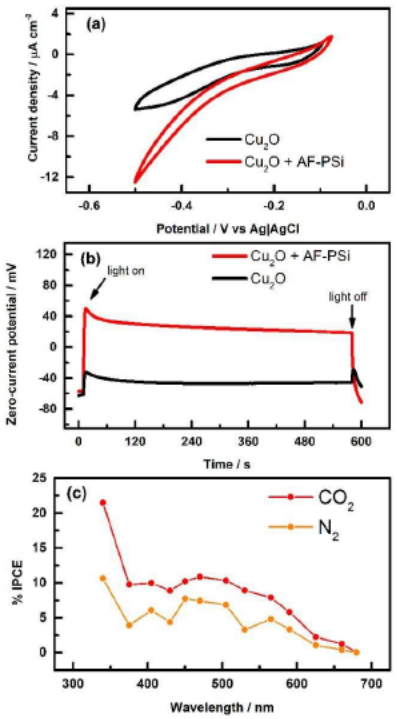


**Figure 1.** Cyclic voltammetry in the dark, 20 mV $s^{-1}$ (a) and variation of zero current potential by irradiation (b) for bare FTO|$Cu_2O$ and FTO|$Cu_2O$—AF—PSi electrodes in $CO_2$-saturated aqueous 0.2 mol $L^{-1}$ $Na_2SO_4$ solution; IPCE curves of FTO|$Cu_2O$-AF-PSi electrode polarized at −0.3 V (vs Ag|AgCl) in $CO_2$- (or $N_2$)-saturated electrolyte (c). For all the measurements, solution pH~7.

Activity of bare $Cu_2O$, $Cu_2O$| AF—PSi and $Cu_2O$| PDMS photoelectrodes towards PEC CO2RR were evaluated by 2 h electrolysis performed under potentiostatic control at —0.3 V (vs Ag/AgCl - see conversion procedure to RHE in Supporting Information), a potential that assures $CO_2$ consumption and minimizes hydrogen evolution reaction in 0.2 M $Na_2SO_4$ aqueous electrolyte (experimental details in Supporting Information). HPLC analysis identified formate as the only product in solution, with 61 % faradaic efficiency when AF—PSi is present at $Cu_2O$ photocathode surface. Also, no gaseous products were identified in the cell atmosphere analyzed by GC-TCD . Also, no product was detected when bare FTO |$Cu_2O$ or FTO| $Cu_2O$| PDMS electrodes were used, which further supports the role of N-containing group in activating $CO_2$ for PEC CO2RR (HPLC chromatograms of all electrolyses in Figure S2a-d).

Electrodes used on electrolyses were analysed by X-ray diffraction (XRD) to evaluate the extent of photocorrosion (Figure 2a). As expected, bare $Cu_2O$ suffered severe photocorrosion (Figures 1a and 1b), with most of the original oxide being converted to metallic copper, in accordance with Equation 1. $Cu_2O$—AF—PSi on the other hand, remains mostly as the original oxide, with $Cu^0$ formation only to a small extent. The same is observed for $Cu_2O$-PDMS, further confirming the photocorrosion inhibition provided by the hydrophobicity of polysiloxanes. The results so far indicate that the benefits provided by AF—PSi to $Cu_2O$ photocathodes can be decoupled as enhanced photostability from polysiloxane backbone and formate selectivity due to amine-containing side chains. Scanning electron microscopy images of bare $Cu_2O$ (non-protected) before and after electrolysis are shown in Figures 2b and 2c, respectively.

To get further insights from these interactions, *in situ* Fourier Transform Infrared Spectroscopy (FTIR) was used to probe the electrode-electrolyte interface of $Cu_2O$ photocathodes. For these experiments, $Cu_2O$ was electrodeposited on stainless steel rods (Figure S3a-c), which were used as working electrodes in a photoelectrochemical cell for *in situ* FTIR measurements (complete setup described elsewhere).[25]

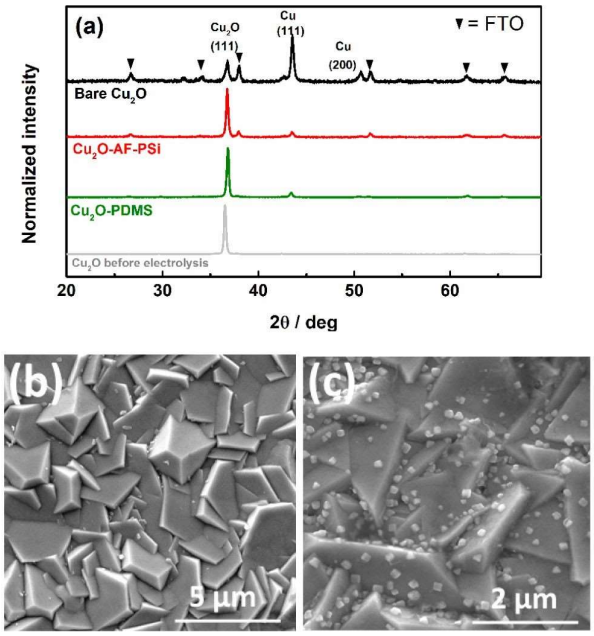


**Figure 2.** Effects of two-hours electrolysis in photocathodes of $Cu_2O$ electrodeposited on FTO, at −0.3 V (vs Ag|AgCl) under 1 Sun illumination: XRD patterns after electrolysis for bare FTO/$Cu_2O$ and electrodes modified with an overlayer of PDMS and AF-PSi; XRD for bare FTO/$Cu_2O$ before electrolysis is also shown for comparison (a). SEM images of bare FTO/$Cu_2O$ (not protected by aminosilane) before (b) and after electrolysis (c).

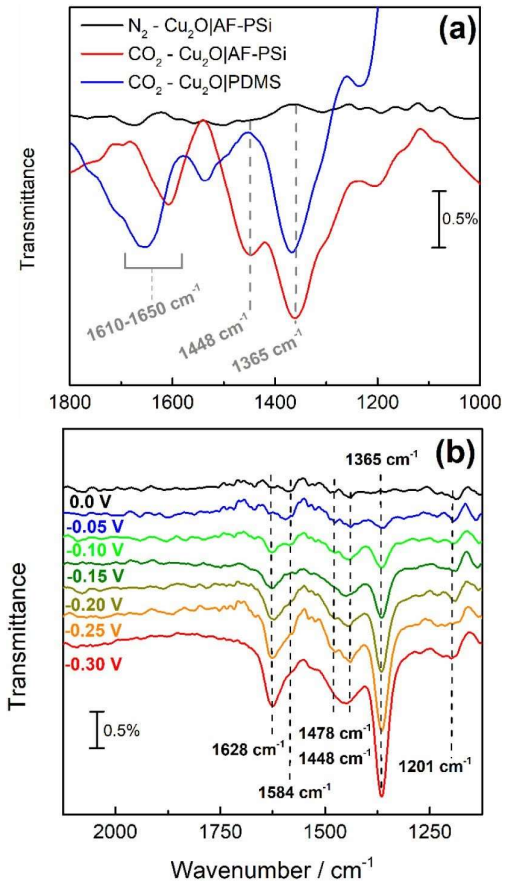


**Figure 3.** *In situ* FTIR experiments performed at the surface of $Cu_2O$/AF-PSi electrode immersed in 0.2 M $Na_2SO_4$ ($D_2O$) electrolyte. (a) comparison between $N_2$- and $CO_2$-saturated electrolyte in the wavenumber range of characteristic carbamate bands. (b) Spectra acquired at illuminated electrode polarized at different potentials in $CO_2$ saturated solution. For all the measurements, solution pH ~ 7. Potentials are *vs.* Ag|AgCl|KCl 3 M – conversion to RHE in S.I.

The influence of amine side chains was investigated in a set of experiments performed with $Cu_2O$|AF-PSi and $Cu_2O$|PDMS electrodes in $Na_2SO_4$ 0.2 M solution in both $D_2O$ and $H_2O$ ($D_2O$ measurements guarantees enhanced sensibility, considering $H_2O$ vibrational spectrum strongly overlaps with the expected bands in the observed region (1800–1000 $cm^{-1}$). First, each electrode was kept at open circuit potential and the solution was saturated with $N_2$, a condition taken as background before $CO_2$ was added to the solution; then, after $CO_2$ saturation, the infrared spectrum of electrode surface was acquired. Figure 3a shows the resulting FTIR spectrum in $D_2O$ electrolyte, with the characteristic bands of the expected compounds, namely carbamate and bicarbonate/carbonate (from $CO_2$ dissolution equilibrium). The bands at 1600–1650 $cm^{-1}$ have been described in the literature as characteristics of both carbamate[16,17] and bicarbonate[26] and cannot be conclusive for carbamate formation solely by literature comparison. The band at 1365 $cm^{-1}$ is associated to C=O stretching of bicarbonate ions in solution[26] and appears at the surface of both AF-PSi and PDMS-covered electrodes. The band at 1448 $cm^{-1}$, however, appears only at the amine-bearing surface, which suggests it is associated to carbamate formation. Bands in the 1400–1460 $cm^{-1}$ range has been reported as indicative of carbamate groups formed in similar polymers to that used in this work.[16,17]

Figure 3b shows FTIR spectra collected from $Cu_2O$|AF-PSi photocathode under illumination during chronoamperometry measurements at different potentials. All the bands observed in this region increases as the electrode is driven to more negative potentials. The electric current associated to each spectrum is shown in Figure S4.

To attribute the bands to chemical species, reference infrared spectra of standards in $Na_2SO_4$ solution were taken using attenuated total reflectance (ATR) technique. Spectrum of sodium bicarbonate solution in $D_2O$ (Figure S5a) shows well-defined bands at 1628 and 1365 $cm^{-1}$, confirming the presence of the ion in the results showed in Figure 3. Sodium formate (Figure S5b) most intense band is observed between 1580–1590 $cm^{-1}$. An additional, less intense band is observed at 1201 $cm^{-1}$ in $D_2O$. These results, together with HPLC experiments confirm that IR bands at 1584/1200 $cm^{-1}$ can be attributed to formate in Figure 3b. These results stress the importance of obtaining the spectra of the standards in the same condition than in the photoelectrochemical experiments. The acid-base equilibria of these species explain the differences in the spectra in the literature for these and many other molecules.

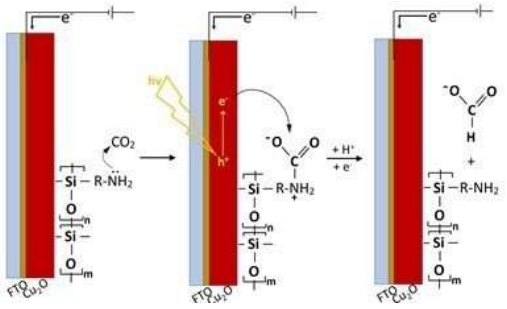

**Scheme 2.** Aminosilane-mediated CO2RR towards formate via carbamate intermediate on $Cu_2O$ photoelectrodes.

To further confirm the attribution of bands to carbamate/bicarbonate, two additional experiments were performed for comparison. The spectra of $Cu_2O$| AF—PSi electrode submitted to the same set of chronoamperometries in $N_2$-degassed electrolyte (to assure the absence of $CO_2$) shown in Figure S6a remained unaltered in the 1800–1000 $cm^{-1}$ wavenumber range. Also, in Figure S6b for irradiated $Cu_2O$ |PDMS electrode, in the presence of $CO_2$, both bands attributed to bicarbonate follow the same behaviour observed for $Cu_2O$| AF—PSi. However, the band previously observed at 1448 $cm^{-1}$, was not observed, further confirming that an amine-$CO_2$ adduct is responsible for its appearance. Thus, considering these observations with HPLC results from electrolysis experiment, where no formate was produced by $Cu_2O$| PDMS electrode, we can confirm that $CO_2$-to-formate reaction at $Cu_2O$ |AF—PSi electrode occurs via carbamate intermediate.

ATR spectrum of AF—PSi under $CO_2$ saturation was obtained using $N_2$-bubbled resin as background (Figure S7). A broad set of band arises at 1400–1450 $cm^{-1}$ after 4 minutes of $CO_2$ bubbling, suggesting that these are related to carbamate formation, and explaining the differences observed in Figure 3b for the results obtained with $Cu_2O$—AF—PSi (containing amino groups able to form carbamate) and $Cu_2O$| PDMS (not expected to form carbamate).

To decouple the effect of light incidence and applied potential, the same experiments showed in Figure 3b were performed in the dark. As shown in Figure S8a, bicarbonate bands at 1628 and 1365 $cm^{-1}$ increases to a much less extension, while the band associated with carbamate (1448 $cm^{-1}$) increases as in the illuminated experiment. The resulting spectra at —0.3 V vs Ag| AgCl of illuminated and dark experiments are shown overlayed in Figure S8b. It is worth noticing that the formation of carbamate takes place at open circuit potential and then further increases induced by electric bias, which at least to our knowledge, is shown in this work for the first time.

*In situ* FTIR spectra of $Cu_2O$|AF—PSi electrode under illumination in the presence of $CO_2$ were also collected in aqueous $Na_2SO_4$ electrolyte. As shown in Figure S9, a complex set of bands arise at negative potentials, the most prominent at 1365 $cm^{-1}$, which was already attributed to bicarbonate anion. The most intense band of bicarbonate at 1628 $cm^{-1}$ could not be observed, as it overlaps with $H_2O$ bands which appears as a broad negative band. The same experiment was performed without illumination from the solar simulator, and only small, inconclusive changes were observed in the same potential range (Figure S10).

In conclusion, we showed that a polysiloxane containing amines as side chains (AF—PSi) provided photostability and $CO_2$-to-formate selectivity to $Cu_2O$ electrodes used for PEC CO2RR. Electrolyses carried out at —0.3 V *vs* Ag| AgCl produced formate (61 % F.E) with almost no photocorrosion when AF—PSi is used as a protective layer, the opposite of bare $Cu_2O$. *In situ* FTIR experiments confirmed the formation of amine-$CO_2$ adduct, which lowers the energetic barrier for electron transfer to $CO_2$ and can then be converted to formate by the well-established one-proton, two-electrons route[27] (Scheme 2). The same experiments showed that carbamate formation is further induced by electric potential. The use of an aminopolysiloxane dual-function overlayer in PEC CO2RR photocathodes fits well within the current demand for improving selectivity and overall viability of photoelectrocatalytic systems.[10,15] Further experiments must be performed to optimize the electrode composition in order to tune the electrode activity, the reaction selectivity and the protection efficiency, namely: i) the procedure to deposit the overlayer can be optimize to tune the film thickness and homogeneity and ii) considering the participation of the polymer in the reaction mechanism, its structure can be tuned by modifying the organic residue and/or the nature of the amino-group.

## *Acknowledgements*

*The authors gratefully acknowledge support from CNPq, FAPESP (the São Paulo Research Foundation, Process 2017/11986-5, 2018/20952-0) and Shell and the strategic importance of the support given by ANP (Brazil's National Oil, Natural Gas and Biofuels Agency) through the R&D levy regulation.*

## *Conflict of Interest*

The authors declare no conflict of interest.

**Keywords:** $CO_2$ reduction · photoelectrochemistry · solar fuels · $Cu_2O$ · *in situ* FTIR

[1] Y. J. Jang, J. S. Lee, *ChemSusChem* **2019**, *12*, 1835–1845.
[2] J. F. de Brito, A. R. Araujo, K. Rajeshwar, M. V. B. Zanoni, *Chem. Eng. J.* **2015**, *264*, 302–309.
[3] J.-C. Wang, L. Zhang, W.-X. Fang, J. Ren, Y.-Y. Li, H.-C. Yao, J.-S. Wang, Z.-J. Li, *ACS Appl. Mater. Interfaces* **2015**, *7*, 8631–8639.
[4] K. Kobayashi, S. N. Lou, Y. Takatsuji, T. Haruyama, Y. Shimizu, T. Ohno, *Electrochim. Acta* **2020**, *338*, 135805.
[5] C. Li, T. Hisatomi, O. Watanabe, M. Nakabayashi, N. Shibata, K. Domen, J.-J. Delaunay, *Appl. Phys. Lett.* **2016**, *109*, 033902.
[6] C. Y. Toe, J. Scott, R. Amal, Y. H. Ng, *J. Photochem. Photobiol. C* **2019**, *40*, 191–211.

[7] I. A. Rutkowska, E. Szaniawska, J. Taniewicz, A. Wadas, E. Seta, D. Kowalski, P. J. Kulesza, *J. Electrochem. Soc.* **2019**, *166*, H3271–H3278.
[8] S. Oh, H. Kang, W. Joo, Y. Joo, *ChemCatChem* **2020**, *12*, 5185–5191.
[9] Y. Li, X. Zhong, K. Luo, Z. Shao, *J. Mater. Chem. A* **2019**, *7*, 15593–15598.
[10] R. Beranek, *Angew. Chem. Int. Ed.* **2019**, 16724–16729.
[11] A. B. Bocarsly, Q. D. Gibson, A. J. Morris, R. P. L'Esperance, Z. M. Detweiler, P. S. Lakkaraju, E. L. Zeitler, T. W. Shaw, *ACS Catal.* **2012**, *2*, 1684–1692.
[12] N. Hollingsworth, S. F. R. Taylor, M. T. Galante, J. Jacquemin, C. Longo, K. B. Holt, N. H. De Leeuw, C. Hardacre, *Angew. Chem. Int. Ed.* **2015**, *54*, 14164–14168; *Angew. Chem.* **2015**, *127*, 14370–14374.
[13] L. Sun, G. K. Ramesha, P. V. Kamat, J. F. Brennecke, *Langmuir* **2014**, *30*, 6302–6308.
[14] W. Lu, B. Jia, B. Cui, Y. Zhang, K. Yao, Y. Zhao, J. Wang, *Angew. Chem. Int. Ed.* **2017**, *56*, 11851–11854; *Angew. Chem.* **2017**, *129*, 12013–12016.
[15] D. Nam, P. De Luna, A. Rosas-hernández, A. Thevenon, F. Li, T. Agapie, J. C. Peters, O. Shekhah, M. Eddaoudi, E. H. Sargent, *Nat. Mater.* **2020**, *19*, 266–276.
[16] T. Yu, K. Wakuda, D. L. Blair, R. G. Weiss, *J. Phys. Chem. C* **2009**, *113*, 11546–11553.
[17] F. S. Mohammed, S. Wuttigul, C. L. Kitchens, *Ind. Eng. Chem. Res.* **2011**, *50*, 8034–8041.
[18] T. D. Golden, M. G. Shumsky, Y. Zhou, R. A. VanderWerf, R. A. Van Leeuwen, J. A. Switzer, *Chem. Mater.* **1996**, *8*, 2499–2504.
[19] C. M. Jiang, G. Segev, L. H. Hess, G. Liu, G. Zaborski, F. M. Toma, J. K. Cooper, I. D. Sharp, *ACS Appl. Mater. Interfaces* **2018**, *10*, 10627–10633.
[20] M. G. Walter, E. L. Warren, J. R. McKone, S. W. Boettcher, Q. Mi, E. A. Santori, N. S. Lewis, *Chem. Rev.* **2010**, *110*, 6446–6473.
[21] U. Kang, S. K. Choi, D. J. Ham, S. M. Ji, W. Choi, D. S. Han, A. Abdel-Wahab, H. Park, *Energy Environ. Sci.* **2015**, *8*, 2638–2643.
[22] S. Kamimura, N. Murakami, T. Tsubota, T. Ohno, *Appl. Catal. B* **2015**, *174–175*, 471–476.
[23] J. Gu, A. Wuttig, J. W. Krizan, Y. Hu, Z. M. Detweiler, R. J. Cava, A. B. Bocarsly, *J. Phys. Chem. C* **2013**, *117*, 12415–12422.
[24] A. D. Handoko, J. Tang, *Int. J. Hydrogen Energy* **2013**, *38*, 13017–13022.
[25] J. L. Bott-Neto, M. V. F. Rodrigues, M. C. Silva, E. B. Carneiro-Neto, G. Wosiak, J. C. Mauricio, E. C. Pereira, S. J. A. Figueroa, P. S. Fernández, *ChemElectroChem* **2020**, *7*, 4306–4313.
[26] M. Baldassarre, A. Barth, *Analyst* **2014**, *139*, 2167–2176.
[27] D. W. Cunningham, J. M. Barlow, R. S. Velazquez, J. Y. Yang, *Angew. Chem. Int. Ed.* **2020**, *59*, 4443–4447.